Article:

Pitts, AD, Casciano, CI, Patacci, M orcid.org/0000-0003-1675-4643 et al. (3 more authors) (2017) Integrating traditional field methods with emerging digital techniques for enhanced outcrop analysis of deep water channel-fill deposits. Marine and Petroleum Geology, 87. pp. 2-13. ISSN 0264-8172

https://doi.org/10.1016/j.marpetgeo.2017.05.001

Accepted Manuscript

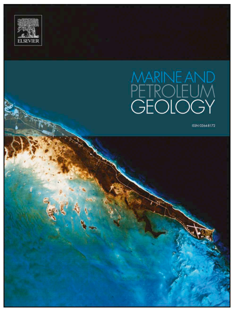

Integrating traditional field methods with emerging digital techniques for enhanced outcrop analysis of deep water channel-fill deposits

Alan Pitts, Claudio Casciano, Marco Patacci, Sergio Longhitano, Claudio Di Celma, William McCaffrey

PII: S0264-8172(17)30160-5

DOI: 10.1016/j.marpetgeo.2017.05.001

Reference: JMPG 2893

To appear in: *Marine and Petroleum Geology*

Received Date: 30 August 2016

Revised Date: 8 April 2017

Accepted Date: 1 May 2017

Title Page

Title

Integrating traditional field methods with emerging digital techniques for enhanced outcrop analysis of deep water channel-fill deposits

Authors

Alan Pitts [a], Claudio Casciano [a], Marco Patacci [b], Sergio Longhitano [c], Claudio Di Celma [a], William McCaffrey [b]

[a] Dipartimento di Scienze della Terra, Università degli Studi di Camerino, Via Gentile III da Varano 1, 62032 Camerino (MC), Italy

[b] Turbidites Research Group, School of Earth and Environment, University of Leeds, Leeds LS2 9JT, UK

[c] Dipartimento di Scienze Geologiche, Università degli Studi della Basilicata, Campus di Macchia Romana, 85100 Potenza, Italy

Corresponding Author

Alan Pitts – pitts.alan@gmail.com

Abstract

The development of emerging digital technologies that allow the collection and analysis of field data represents a significant innovation in field-based geological studies. The integration of these digital techniques to traditional sedimentological field methods determines considerable improvements in outcrop characterization of ancient successions. An example of this integrated modern approach for geological data collection is employed for the detailed characterization of a turbidite channel-lobe system of the Gorgoglione Flysch Formation in Southern Italy. The studied section, exposed above the village of Castelmezzano, has been measured and described in detailed stratigraphic sections, providing data for both sedimentological analysis and correlation of the stratigraphy. In order to gain a complete perspective on the exposure and stratigraphic elements, analysis of physical outcrop data was enhanced by the use of high-resolution Gigapixel imagery and 3D photogrammetric outcrop reconstructions. The Santa Maria section has been assessed in terms of vertical and lateral facies stacking arrangements and subdivided into two component facies associations separated by a prominent concave-up erosional boundary. The lower facies association, interpreted as a frontal lobe complex, consists of tabular, thick-bedded coarse sandstones interbedded with persistent heterolithic packages of thin-bedded sandstones and mudstones, and minor soft-sediment deformed strata. The upper facies association represents the infill of a channel-form and consists of a basal conglomerate, passing gradually upwards into massive amalgamated sandstones overlain by large-scale cross-laminated sandstones. The excellent exposure of the Santa Maria section records the complete evolution of a channel-lobe system, transitioning from frontal lobe deposition through channel incision and bypass, to progressive backfilling. This study shows how facies characterization, stratigraphic correlations and reconstruction of the depositional architectures have been substantially enhanced by the use of emerging digital techniques for geological data collection.

1. Introduction

The improved capabilities of Gigapixel imagery systems and 3D photogrammetry software suites in recent years provide useful tools that can strengthen traditional stratigraphic field data. Gigapixel imagery systems are able to record very high resolution photomosaics, which allow an unprecedented level of inspection of outcrops, while photogrammetry software, such as Agisoft Photoscan allows 3D outcrop reconstructions from ground-based or aerial photos to be manipulated and viewed from multiple angles. These tools can fill critical gaps in stratigraphic data by permitting the inspection of both bed-scale and outcrop-scale details from distances and angles unachievable in person.

Turbidite channels are one of the most important pathways for sediment transport into ocean basins and their sedimentary infill has proven to be one of the most common types of hydrocarbon reservoirs found in deep water settings (e.g. Mayall et al., 2006). Seismic stratigraphy applied to conventional and high-resolution three-dimensional (3D) data sets offered a compelling method to understanding their internal stratal and architectural complexity (Mayall and Stewart, 2000; Posamentier and Kolla, 2003; Deptuck et al., 2003). However, a high degree of spatial variability of reservoir properties is associated with differences in the nature of channel fill and their stacking patterns occurring at scales below the resolution of 3D seismic datasets. Over the past years, to improve the sub-seismic characterization of submarine channel fills, numerous studies have focused on the details of suitable outcrop analogues, greatly improving our knowledge on distribution of sedimentary facies, grain size, and small-scale architectural elements and factors that may control the observed changes in stratigraphic architecture (e.g. Mutti and Normark, 1987; Posamentier et al., 1991; Pickering et al., 2001; Camacho et al., 2002; Brunt and McCaffrey, 2007; Schwarz and Arnott, 2007; Navarro et al., 2007; Kane et al., 2009; Pyles et al., 2010; McHargue et al., 2011; Di Celma et al., 2011; Figueiredo et al., 2013; Hubbard et al., 2014; Bain and Hubbard, 2016). Field methods for data collection, however, have remained the same for nearly the last two hundred years. Considering the rapid state of improvement and increased availability in digital technologies, there is a need to update the traditional techniques by integrating emerging digital field methods (e.g. McCaffrey et al., 2005; Wynn et al., 2005; Thurmond et al., 2006; Nieminski and Graham, 2017).

For this study, we consider a well exposed channel-lobe system from a key stratigraphic interval of the Upper Miocene Gorgoglione Flysch Formation (GFF), a coarse-grained siliciclastic turbidite succession that crops out in the Southern Apennines of Italy (Fig. 1). The studied section, informally named the Santa Maria section, is of primary importance in the interpretation of the stratigraphic evolution of the whole GFF, since it represents one of the best-preserved isolated channels characterizing the upper portion of the turbidite succession (Casciano et al., 2017). This section was analyzed using standard field methods integrated with new digital field methods using a GigaPan imagery system and 3D photogrammetry. The goal of using these additional tools is to develop new methodologies for creating digital outcrop reconstructions that can supplement physical data for enhanced facies characterization of bed-scale architecture and facies distribution. The methods for creating GigaPan and 3D outcrop reconstructions, as well as their utility for research are described in this text. However, they are best seen in their digital format and can be found at a permanent online location at www.geode.net as part of a larger collection of digital geologic materials.

2. Geologic and depositional setting

The Southern Apennine Chain is a fold-and-thrust belt developed from late Oligocene to Pleistocene within the general framework of Africa-Europe major plate convergence on an eastward-retreating, W-dipping subduction zone (Doglioni, 1991; Patacca and Scandone, 2007 and references therein). The resulting north-eastward migration of the thrust front determined the progressive involvement in the thrust belt of several intervening Meso-Cenozoic basin and platform successions covering the Adria passive margin and adjacent Tethyan ocean. Accordingly, the structure of the Southern Apenninic orogenic wedge is configured as a thick thrust pile of heavily deformed rootless nappes, tectonically overlying the subducted Apulian platform carbonates and associated foredeep deposits (Vezzani et al., 2010 and references therein). Thrust-top clastic successions of upper Eocene to Plio-Pleistocene age unconformably cover the whole thrust-pile (Patacca and Scandone, 2007). Among them, one of the better preserved units is the late Burdigalian – early Tortonian GFF (Selli, 1962; Giannandrea et al., 2016). This ~1,950 m thick siliciclastic turbidite succession consists of coarse sandy turbidites and mudstones with subordinate conglomerates, filling a narrow and NNW-SSE oriented wedge-top basin (Boiano, 1997). Primary exposures of the GFF occur along the eastern edge of the former basin, in a 25 km wide outcrop belt, between the towns of Castelmezzano and Gorgoglione, 25 km SE of Potenza (Fig. 1). In this area, the GFF unconformably overlies the Cretaceous - Eocene mud-rich succession of the Argille Varicolori Fm. (Fig. 1; Boiano, 1997). Deposition of the GFF was strictly controlled by the contractional tectonic deformations affecting the Apenninic accretionary wedge (Patacca et al., 1990; Boiano, 1997; Giannandrea et al., 2016). Provenance data shows that the GFF was sourced from a crystalline basement terrane located within the growing orogen to the West (Critelli and Loiacono, 1988). However, paleocurrent data document a prevalent paleoflow direction from NNW to SSE, along the longitudinal axis of the basin (Loiacono, 1974). Consequently, many authors invoked a palaeogeographic scenario with sediment gravity flows initiated from an inferred shelf in the orogenic hinterland, which were directed down a NE-facing paleoslope and were successively deviated toward SSE along the basin axis near the base of slope (Boiano, 1997).

In the Castelmezzano – Pietrapertosa area, the lower ~ 1200 m of the succession are characterized by the occurrence of amalgamated sandbodies up to 25 m thick, systematically stacked to form extensive channel complex sets. A ~ 700 m thick clay-prone succession incised by isolated arenaceous-conglomeratic channels constitutes the topmost part of the basin-fill succession, where the studied section is located. The vertical architectural and grain-size evolution of channel types documented in the upper 1000 m of the turbidite succession (from amalgamated sand-filled channels to isolated conglomerate-rich channels), together with the gradual upward change in the background sedimentation (from sand-prone to clay-prone heterolithic deposits), likely reflects a shift along the depositional profile, passing from a near base-of-slope to a slope setting as a result of slope progradation (Casciano et al., 2017).

3. Methodology

The Santa Maria section was recorded and measured using both traditional sedimentary facies analysis data collection and emerging digital field techniques for outcrop mapping and data collection. Traditional methods included bed-scale characterization of sedimentological and stratigraphic elements and a paleoflow analysis. Stratigraphic data were collected in 8 measured sections logged at centimeter resolution, recording grain size distribution, bed thickness, internal bedding divisions, and bounding surfaces. Paleoflow data were recorded from 361 basal paleoflow indicators, such as flutes and grooves, and cross bed stratification. Additional digital data collection methods included the construction of ultra-high resolution outcrop panoramas produced by the GigaPan® imagery system and 3D outcrop models obtained from aerial and ground based imagery using structure-from-motion (SFM) 3D photogrammetry to aid in identification of key surfaces and the depositional architectures of stratigraphic units. The GigaPan image system is a tripod mounted robotic device, which functions with both point-and-shoot or DSLR cameras, and guides the camera through precise photo grid with each photo at the maximum zoom level. The resulting photo set is stitched together using GigaPan Stitch® software to render a massive photomosaic image built from hundreds of individual photos (Fig. 2). The resulting images are viewed in the GigaPan® viewer or on their online site, www.gigapan.com, as “tiled” dynamic images in which the resolution increases at deeper levels of zoom. The GigaPan® device was used at four key locations for recording the section, two medium-range positions to record outcrop sections and two close-range positions to record detailed bed-scale features of two basal surfaces showing large numbers of scour structures (Fig. 2A). Our methods for creating 3D outcrop models involved large numbers of overlapping photos acquired from multiple positions and angles from the outcrop, taking advantage of all available ground-based viewpoints of the exposure. Photos were taken from unoriented positons and varying distances from the outcrop within approximately 50 m, maintaining photo overlap at values greater than 50%. An aerial-based photo set was acquired under the same general procedure from a helicopter above the study area. The photos were processed using Agisoft Photoscan® software to produce 3D outcrop models (Fig. 3). Physical outcrop and GigaPan data sets were merged together by converting the large GigaPan images from their propriety GigaPan format into a static image format such as Photoshop RAW or TIFF at maximum resolution. The reformatted images were carefully annotated at full scale, transcribing the measured stratigraphic data directly on to the images recording centimeter scale features (Fig. 4). Correlations of stratigraphic intervals and surfaces were made directly onto the annotated GigaPan image supported by the use of the 3D outcrop models to verify interpretations.

4. Results

The studied interval of the Santa Maria section is approximately 40 m high and 280 m wide. In the following paragraphs, the results obtained from the analysis of physical and digital outcrop data are presented.

4.1. Sedimentary Facies and Facies Associations

At the smallest scale, sedimentary units are represented by beds, indicating a single sedimentation event. They are recognized as the products of gravity flow processes, based on bed-scale characteristics (cf., Bouma, 1962; Lowe, 1982, Talling et al. 2012). Six facies, grouped in two major sedimentary facies associations, have been distinguished in the Santa Maria section (Figs. 5, 6). Their detailed description, lateral and vertical distribution, and process-based interpretation are provided in Table 1.

4.1.1. Facies Association A

Description: Facies association A has been observed in the lower portion of the studied section (Figs. 5, 6). It is composed of three main facies: a medium to thick bedded sandstone (facies A1), heterolithic packages of interbedded mudstone and thin-bedded fine grained sandstones (facies A2), and isolated zones of highly convoluted and contorted sandstone beds (facies A3). Facies A1 (Fig. 7A, B) is found at the base of the section with beds stacked forming 1-3 m thick bed-sets with sharp upper and lower contacts. Paleocurrent indicators from sole structures exposed along basal A1 surfaces, such as flute casts and grooves, display a range of variability between SW and SE (Fig. 6). Observations from aerial panoramic photos reveal that A1 sandstone beds gradually thin toward NNE over several hundred meters, displaying an apparent lenticular geometry. Sandstone packages of facies A1 are punctuated by thin, laterally continuous packages of facies A2 (Fig. 7C), displaying a constant thickness throughout the entire exposure. Facies A3 is found as isolated wedge-shaped intervals of intrastratal deformation (Fig. 7D), which are laterally equivalent to facies A2. Several ductile and brittle deformation features are observed, including chaotic and disintegrated strata containing folds, de-watering structures and minor displacements of dismembered bedding along basal thrust planes. Deformation zones are bound below and above by stratified sand beds of facies A1, with underlying beds showing gently sheared bedforms. Upper bounding surfaces of deformation zones are found as sharp contacts with overlying beds of undisturbed bedding.

Interpretation: Based on sedimentary structures, bedding geometry and paleoflow dispersion, sand rich packages of facies A1 are interpreted as individual lobes stacked vertically to form a lobe complex (Prélat et al., 2009). The wide range of paleoflow dispersion documented from sole structures indicates deposition in a loosely confined environment. These lobes are intercalated with the heterolithic packages of facies A2, interpreted as interlobe deposits regarded as part of distal lobe fringes (Prélat and Hodgson, 2013). Intrastratal deformation zones described in facies A3 and found in this section as well as several other nearby sections within the GFF, are interpreted as slump intervals. These slumps are possibly triggered in association with margin failures of the contemporaneous feeder channel, located up dip of the depositional lobes. Locally, thrust bound sandstone beds with mildly deformed laminae beneath occurring within the slump zones, show evidence of composite deformation across the lower boundary of the slump interval (Butler and McCaffrey, 2010). These deformed deposits are restricted to the heterolithic facies A2 and triggered along basal detachment planes in mud-rich mechanically "weak" layers. The presence of these deformational features limited to specific lithofacies indicates the direct influence of depositional architecture on the location and size of slope failure and intrastratal deformation (Auchter et al., 2016).

4.1.2. Facies Association B

Description: Facies association B (Fig. 8) has been documented in the upper portion of the Santa Maria section, directly overlying the deposits of facies association A. Facies association B reaches a maximum thickness of 17.5 m and is composed of three primary facies: a basal chaotic polymictic conglomerate in a coarse-grained sandstone matrix (facies B1), passing gradually upwards into massive amalgamated sandstones (facies B2), and large-scale cross-laminated sandstones in the upper-most portion (facies B3). The first two facies are laterally confined within an irregularly-shaped, concave-upward erosional surface deeply incised into the underlying deposits of facies association A. This surface can be traced for approximately 1.2 km along the outcrop (Fig. 5B). It has a pronounced meter-scale "step and flat" geometry (Figs. 5C, 6) with the "flat" segments in most cases eroding along parallel surfaces to the underlying bedding and the "step" portions rising abruptly vertically across sandstone beds before arching back along the bedding, forming the next step. Step-up surfaces are found to stratigraphically correspond with vertical grain-size jumps and secondary erosional surfaces in the coarse-grained conglomerate of facies B1. Basal conglomerates of facies B1 rest directly above the erosional surface and show subtle normal grading with several fining-upward sequences and minor erosional surfaces. The coarsest B1 material is found within the deepest and central portion of the erosional surface and is composed of large rounded and angular extra-basinal clasts up to 80 cm mixed with rip-up mud clasts (Fig. 8A). The abundance of extra-basinal clasts decreases with lateral distance from the central part of the section gradually being replaced by mud rip-up clasts before eventually disappearing altogether (Fig. 8B). Paleocurrent indicators from sole marks measured along the base of facies B1 (Fig. 8C), show a NW-SE trend with a limited range of dispersion. Amalgamated sandstones of facies B2 (Fig. 8D) show normal grading, with bedding indicated by horizons of irregularly-shaped mud clasts that amalgamate and bifurcate over short distances. In the thicker central portion of the section, amalgamated sandstones (facies B2) directly overlie basal conglomerates (of facies B1), whereas in lateral positions they are found draping the erosional surface. Cross-laminated sandstones of facies B3 (Fig. 8E) show an abrupt transition from underlying amalgamated sands with thickness varying from 1 to 3 m. Facies B3 occurs as a "capstone" interval, which is distributed across the entire exposure and present in all measured sections. The cross stratification displays a highly variable pattern of paleocurrent directions, diverging up to 75° towards SW from the paleoflow documented from the sole structures.

Interpretation: Based on vertical and lateral facies stacking arrangements, facies association B is interpreted as the infill of a single channel-form. The stepped-terrace geometry and multiple internal erosion surfaces have been recognized by other authors in similar slope channel systems (e.g. Eschard et al., 2003; Navarro et al., 2007; Hubbard et al., 2014) and indicate the composite nature of the basal surface. The basal conglomeratic interval (facies B1) is associated with erosional phases and substantial sediment bypass. The relative abundance of extra-formational conglomeratic clasts in the deepest and central portion of the erosional surface indicates the channel axis, where flow velocity was highest (McHargue et al., 2011; Stevenson et al., 2015). Conversely, their absence in lateral portions of the section, with a concurrent increase of mud-rich conglomerates, indicates channel off-axis (Fig. 9A). Because the gravelly facies B1 may represent only a small fraction of the total sediment load in large, turbulent sediment gravity flows, the preservation of thick, amalgamated gravelly packages implies that much greater amounts of sand and mud have completely bypassed the study area during its deposition. As such, this type of basal coarse-grained material has been recognized as a typical bypass facies (e.g. Alpak et al, 2013; Di Celma et al., 2013; Stevenson et al., 2015) draping the basal erosion surface. Amalgamated sandstones of facies B2 are interpreted as the product of rapid suspension deposition by sand-rich turbidity currents during the backfilling phase of the channel-form. The large-scale cross-laminated sandstones of facies B3 are interpreted as indicating the loss of channel confinement. Divergent paleoflow between basal sole structures (~ 140°) and upper cross stratification (up to ~ 220°) is consistent with lateral flow expansion as channel confinement progressively decreases. Similar facies patterns have been described by Schwarz and Arnott (2007) in the Isaac Formation of the Windermere Supergroup of Canada in channel fills capped by dune-cross-stratified sandstones. The occurrence of amalgamated coarse-grained sandstones capped by cross-laminated sandstones has been recognized in many other channel-fill deposits of the GFF, constituting a recurring motif in the process of channel infilling at the basin scale.

4.2 Channel Dimensions and Hierarchy

The Santa Maria exposure is oriented in a N-S direction, highly oblique to the primary channel paleoflow direction inferred from the measurements of the basal structures. For this reason, the aspect ratio (width: thickness) of the Santa Maria channel has been calculated for a reconstructed strike-oriented cross sections by projecting the apparent dimensions onto a surface normal to the average paleocurrent direction. Using this method, the actual width of the channel is calculated at about 180 m. Comparable dimensions for channel-fill deposits are reported in literature for other deep-water systems (e.g. McHargue et al., 2011; McHauley and Hubbard, 2013; Figueiredo et al., 2013; Stright, et al. 2014). By using the scheme proposed by Pemberton et al. (2016) the dimensions of the Santa Maria channel (180 m wide and 17.5 m thick) are consistent with a low-aspect-ratio channel. According to the hierarchical scheme of Campion et al. (2005), this channel is defined as a single channel element.

5. Discussion

5.1. Evolution of Santa Maria channel-lobe depositional system

The deposits exposed along the Santa Maria section record the complete lifespan of a channel-lobe system, with deposition passing from frontal lobe growth, through channel incision, to confined backfilling and eventual spillover (Figs. 9A, 9B). The analyzed channel-lobe system, with the channel erosionally overlying frontal lobes, displays a characteristic stacking pattern that has been recently documented in ancient and modern settings (Morris et al., 2014; Hodgson et al., 2016).

5.1.1 Deposition of frontal lobes

The sand-rich tabular strata underlying the Santa Maria channel indicate the deposition of frontal lobes (Fig. 9B) in unconfined settings down-dip of the feeder channel, by numerous individual high-energy sediment gravity flows (Prélat et al., 2009). The laterally-continuous heterolithic interlobes and the wide range of paleoflow dispersion show that depositional lobe emplacement was migrating positions as lobes avulsed seeking accommodation space (Prelat and Hodgson, 2013).

5.1.2 Initiation of channel form and erosional surface

The incisional relationship between channel and lobe deposits indicates that the Santa Maria channel initiated with excavation of the seafloor by highly-energetic sedimentary gravity flows as the channel advanced over the lobe (Fig. 9B; Fildani et al., 2013). This process is recognized as result of slope channel lengthening occurring in tandem with the simultaneous deposition of new frontal lobes down dip (Morris et al., 2014). During this period, the channel functioned as conduit for sediment transfer with a majority of sediment flowing to a down dip depocenter (Hubbard et al., 2014). This phase of the channel initiation has been recognized as a period of maximum bypass-lag deposition (Eschard et al, 2003; McHargue et al., 2011; Stevenson et al., 2015). The protracted passage of high-energy turbidity flows caused the repeated erosion of the substrate that sculpted the irregular basal channel-form, characterized by a “step-and-flat” geometry, mantled by coarse-grained lag material. Stratigraphic correlations between “flat” segments in the channel base geometry and significant grain size jumps and secondary erosional surfaces with in the lag deposits confirm these multiple incisional phases, with gravity flows eroding and reworking the lag deposits during each successive event.

5.1.3 Backfilling of the Santa Maria Channel

After the complex incisional phase that sculpted the irregular channel form, the Santa Maria channel was almost completely filled by sandy sediments, during a period referred to as backfilling (Gardner and Borer, 2000; Fig. 9). This phase is indicated by the presence of the massive amalgamated sandstones of facies B2. These sandstones suggest deposition in a confined channel under waning flow conditions favoring rapid fallout of sediment with minor incision into the substrate. The frequency of aligned mud clast intervals marking multiple amalgamation surfaces, suggests that the filling of the channel was achieved through many successive events.

5.1.4 Loss of confinement

The presence of laterally-persistent cross-laminated sandstone of facies B3 capping the channel-fill sequence suggests a transition from confined to poorly-confined conditions as the channel became filled with partially-overspilling turbidity currents (Fig. 9B).

6. Conclusions

Integration of digital outcrop data with traditional stratigraphic field techniques, has significantly improved the reconstruction of the Santa Maria section, increasing the spatial resolution of the geological data and allowing the investigation of inaccessible portions of the outcrops. The use of single GigaPan images allows inspection of the exposure at variable scale, from centimeter scale bedforms up to outcrop-scale stratigraphic architectures. Through the use of 3D outcrop models, the interpretation of the depositional architectures and bedding geometries has been carried out with greater certainty. This study shows how facies characterization and high-resolution stratigraphic correlation can greatly benefit by the use of these emerging digital data collection techniques. The detailed characterization of sedimentary facies distribution and the enhanced analysis of architectural elements at the Santa Maria section allowed the interpretation of the stratigraphic evolution of a submarine channel-lobe system. Facies associations and the discrepancy between paleoflow dispersion patterns indicate two primary depositional settings and a range of flow types, from confined flows occurring in the slope channel to unconfined flows producing frontal lobes downdip of the feeder channel. Multiple phases of the Santa Maria channel evolution have been documented, from channel incision and sediment bypass, to protracted backfilling from high-density turbidity flows recording a progressive loss of confinement. The combined methodology proposed in this paper provides solutions to the challenges involved with outcrop characterization by creating observation points from perspectives and distances that are not physically possible in the field. Furthermore, these digital outcrop reconstructions allow researchers to return from the field with a precise and detailed record of the study area, which can be used to support the verification of additional interpretations during the analysis of data. While this case-study focuses on the applications of this approach as a tool for enhanced sedimentary facies analysis, the methodologies discussed here can be useful in a broad range of geoscience research applications (e.g., for the creation of high-resolution DTM's), particularly where the sole use of traditional field data collection tools is not sufficient to provide a complete perspective of the broad geological context.

Acknowledgements

This work was funded by University of Camerino and Turbidites Research Group industry sponsors: Anadarko, BG-Group, BP, Conoco Phillips, Dana Petroleum, Eni, Nexen, OMV, Petronas, Shell, Statoil and Woodside. We also acknowledge the support of the GEODE group (Google Earth for Onsite and Distance Education) for assistance with the GigaPan and 3D photogrammetry equipment and procedures. The authors thank the reviewers for helping to strengthen this manuscript.

References

Alpak, F.O., Barton, M.D., Naruk, S.J., 2013. The impact of fine-scale turbidite channel architecture on deep-water reservoir performance. AAPG Bulletin, 97, 251–284.

Auchter, N.C., Romans, B.W., Hubbard, S.M. 2016. Influence of deposit architecture on intrastratal deformation, slope deposits of the Tres Pasos Formation, Chile. Sedimentary Geology, 341, 13-26.

Bain, H.A., Hubbard, S.M., 2016. Stratigraphic evolution of a long-lived submarine channel system in the Late Cretaceous Nanaimo Group, British Columbia, Canada. Sedimentary Geology, 337, 113-132.

Boiano, U., 1997, Anatomy of a siliciclastic turbidite basin: The Gorgoglione Flysch, Upper Miocene, southern Italy: physical stratigraphy, sedimentology and sequence-stratigraphic framework. Sedimentary Geology, v. 107, p. 231–262.

Bouma, A.H., 1962. Sedimentology of Some Flysch Deposits; A Graphic Approach to Facies Interpretation. Elsevier, Amsterdam, 168 pp.

Brunt, R.L., McCaffrey, W.D., 2007. Heterogeneity of fill within an incised channel: The Oligocene Gres du Champsaur, SE France. Marine and Petroleum Geology, 24, 529-539.

Butler, R.W.H., McCaffrey, W.D. 2010. Structural evolution and sediment entrainment in mass-transport complexes: outcrop studies from Italy. Journal of the Geological Society, 167, 617-631.

Camacho, H., Busby, C.J., Kneller, B., 2002. A new depositional model for the classical turbidite locality at San Clemente State Beach, California. AAPG Bulletin, 86, 1543–1560

Casciano, C.I., Di Celma, C., Patacci, M., Longhitano, S.G., McCaffrey, W.D., 2017. Hierarchy and facies distribution in turbiditic sandstone channel-fills: the Gorgoglione Flysch Formation (Miocene of Basilicata, Southern Italy). In: Deep-water Depositional Systems: Advances and Applications Conference, 25-27 January, The Geological Society, London, UK.

Ciaranfi, N., 1972. Il Flysch di Gorgoglione. Boll. Serv. Geol. d'It., 92, 101-114.

Critelli, S., & Loiacono, F. (1988). Provenienza e dispersione dei sedimenti nel flysch di Gorgoglione (Langhiano–Tortoniano, Appennino Lucano): Implicazioni sull'evoluzione delle mode detritiche arenacee nell'orogene sudappenninico. Memorie della Società Geologica Italiana, 41, 809-826.

Deptuck, M.E., Sylvester, Z., Pirmez, C., O'Byrne, C., 2007. Migration–aggradation history and 3-D seismic geomorphology of submarine channels in the Pleistocene Benin-major Canyon, western Niger Delta slope: Marine and Petroleum Geology, 24, 406–433.

Di Celma, C., Brunt, R.L., Hodgson, D.M., Flint, S.S. Kavanagh, J.P., 2011. Spatial and temporal evolution of a Permian submarine slope channel-levee system, Karoo Basin, South Africa. Journal of Sedimentary Research, 81, 579-599.

Di Celma, C., Cantalamessa, G., Didaskalou, P., 2013. Stratigraphic organization and predictability of mixed coarse-grained and fine-grained successions in an upper slope Pleistocene turbidite system of the Peri-Adriatic basin. Sedimentology, 60, 763–799.

Doglioni, C., 1991. A proposal for the kinematic modelling of W-dipping subductions-possible applications to the Tyrrhenian□Apennines system. Terra Nova, 3, 423-434.

Eschard, R., Albouy, E., Deschamps, R., Euzen, T., Ayub, A. (2003). Downstream evolution of turbiditic channel complexes in the Pab Range outcrops (Maastrichtian, Pakistan). Marine and Petroleum Geology, 20, 691-710.

Figueiredo, J.J.P., Hodgson, D.M., Flint, S.S., Kavanagh, J.P., 2013. Architecture of a channel complex formed and filled during long-term degradation and entrenchment on the upper submarine slope, Unit F, Fort Brown Fm., SW Karoo Basin, South Africa: Marine and Petroleum Geology, 41, 104–116.

Fildani, A., Hubbard, S.M., Covault, J.A., Maier, K.L., Romans, B.W., Traer, M., Rowland, J.C., 2013. Erosion at inception of deep-sea channels: Marine and Petroleum Geology, 41, 48–61.

Gardner, M.H., Borer, J.M., 2000. Submarine channel architecture along a slope to basin profile, Brushy Canyon Formation, West Texas. In: Bouma, A.H., Stone, C.G. (Eds.), Fine-Grained Turbidite Systems. Memoir 72-American Association of Petroleum Geologists and Special Publication 68-SEPM, pp. 195e214.

Giannandrea, P., Loiacono, F., Maiorano, P., Lirer, F., Puglisi, D., 2016. Geological map of the eastern sector of the Gorgoglione Basin (southern Italy). Italian Journal of Geosciences, 135, 120-141.

Hubbard, S.M., Covault, J.A., Fildani, A., Romans, B.W., 2014. Sediment transfer and deposition in slope channels: Deciphering the record of enigmatic deep-sea processes from outcrop: Geological Society of America Bulletin, 126, 857–871.

Hodgson, D.M., Kane, I.A., Flint, S.S., Brunt, R.L., and Ortiz-Karpf, A., 2016, Time-Transgressive Confinement On the Slope and the Progradation of Basin-Floor Fans: Implications For the Sequence Stratigraphy of Deep-Water Deposits: Journal of Sedimentary Research, v. 86, p. 73–86, doi: 10.2110/jsr.2016.3.

Kane, I.A., Dykstra, M.L., Kneller, B.C., Tremblay, S., McCaffrey, W.D., 2009. Architecture of a coarse-grained channel levée system: the Rosario Formation, Baja California, Mexico. Sedimentology, 56, 2207-2234.

Loiacono, F., 1974. Osservazioni sulla direzione delle paleocorrenti nel Flysch di Gorgoglione (Lucania). Bollettino della Società Geologica Italiana, 93, 1127-1155.

Lowe, D.R., 1982. Sediment gravity flows: depositional models with special reference to the deposits of high-density turbidity currents. Journal of Sedimentary Petrology, 52, 279–297.

Macauley, R.V., Hubbard, S.M., 2013. Slope channel sedimentary processes and stratigraphic stacking, Cretaceous Tres Pasos Formation slope system, Chilean Patagonia. Marine and Petroleum Geology, v. 41, p. 146–162.

Mayall, M., Jones, E., Casey, M., 2006. Turbidite channel reservoirs—Key elements in facies prediction and effective development: Marine and Petroleum Geology, 23, 821–841.

Mayall, M., Stewart, I., 2000. The architecture of turbidite slope channels. In Deep-Water Reservoirs of the World: SEPM, Gulf Coast Section, 20th Annual Research Conference (Vol. 578, p. 586).

McCaffrey, K.J.W., Jones, R.R., Holdsworth, R.E., Wilson, R.W., Clegg, P., Imber, J., Holliman, N., Trinks, I., 2005. Unlocking the spatial dimension: digital technologies and the future of geoscience fieldwork: Journal of the Geological Society, 162, 927–938.

McHargue, T., Pyrcz, M.J., Sullivan, M.D., Clark, J., Fildani, A., Romans, B., Covault, J., Levy, M., Posamentier, H., Drinkwater, N., 2011. Architecture of turbidite channel systems on the continental slope: Patterns and predictions: Marine and Petroleum Geology, 28, 728-743.

Morris, E.A., Hodgson, D.M., Flint, S.S., Brunt, R.L., Butterworth, P.J., Verhaeghe, J., 2014. Sedimentology, stratigraphic architecture, and depositional context of submarine frontal-lobe complexes. Journal of Sedimentary Research, 84, 763–780.

Mutti, E., Normark, W.R., 1987. Comparing Examples of Modern and Ancient Turbidite Systems: Problems and Concepts. In Leggett, J.K., and Zuffa, G.G., eds., Marine Clastic Sedimentology: Springer, The Netherlands, p. 1–38.

Navarro, L., Khan, Z., Arnott, R. W. C., 2007. Depositional architecture and evolution of a deep-marine channel-levee complex: Isaac Formation (Windermere Supergroup), Southern Canadian Cordillera. In: T. H. Nilsen, R. D. Shew, G. S. Steffens, and J. R. J. Studlick, eds., Atlas of deep-water outcrops: AAPG Studies in Geology 56, CD-ROM, 22 p.

Nieminski, N.M., and GRAHAM, S.A., 2017, Modeling Stratigraphic Architecture Using Small Unmanned Aerial Vehicles and Photogrammetry: Examples From the Miocene East Coast Basin, New Zealand: Journal of Sedimentary Research, v. 87, p. 126–132, doi: 10.2110/jsr.2017.5.

Patacca, E., Scandone, P., 1989. Post-Tortonian mountain building in the Apennines. The role of the passive sinking of a relic lithospheric slab. In: Boriani, A., Bonafede, M., Piccardo, G.B., Vai, G.B. (Eds.), The Lithosphere in Italy: Atti Convegno Lincei, 80, pp. 157–176.

Patacca, E., Sartori, R., Scandone, P., 1990. Tyrrhenian basin and apenninic arcs: kinematic relations since late Tortonian times. Memorie della Societ`a Geologica Italiana 45, 425–451.

Patacca, E.,Scandone, P., 2007. Geology of the Southern Apennines. Bollettino della Società Geologica Italiana, 7, 75–119.

Pemberton, E.A.L., Hubbard, S.M., Fildani, A., Romans, B., Stright, L., 2016. The stratigraphic expression of decreasing confinement along a deep-water sediment routing system: Outcrop example from southern Chile: Geosphere, 12, 114–134.

Pescatore, T.S., 1978. Evoluzione tettonica del Bacino Irpino (Italia Meridionale) durante il Miocene. Boll. Soc. Geol. Ital., 97, 783–805.

Pescatore, T.S. and Senatore, M., 1986. A comparison between a present-day (Taranto Gulf) and a Miocene (Irpinian Basin) foredeep of the Southern Apennines (Italy). In: Foreland Basins (Eds P.A. Allen and P. Homewood). Spec. Publ. Int. Assoc. Sediment., 8, 169–182.

Pescatore, T., 1992. La sedimentazione miocenica nell'Appennino campano-lucano. Mem. Soc. Geol. It., 41, 37-46.

Pickering, K.T., Hodgson, D.M., Platzman, E., Clark, J.D. and Stephens, C., 2001. A new type of bedform produced by backfilling processes in a submarine channel, Late Miocene, Tabernas-Sorbas Basin, SE Spain. Journal of Sedimentary Research, 71, 692-704.

Posamentier, H.W., Erskine, R.D., Mitchum, R.M., Jr, 1991. Models for Submarine-Fan Deposition within a Sequence-Stratigraphic Framework, in Seismic Facies and Sedimentary Processes of Submarine Fans and Turbidite Systems, New York, NY, Springer New York, Frontiers in Sedimentary Geology, 127–136.

Posamentier, H.W., Kolla, V., 2003. Seismic geomorphology and stratigraphy of depositional elements in deep-water settings: Journal of Sedimentary Research, 73, 367–388.

Prélat, A., Hodgson, D.M., 2013. The full range of turbidite bed thickness patterns in submarine lobes: controls and implications: Journal of the Geological Society, London, 170, 209–214.

Prélat, A., Hodgson, D.M., Flint, S.S., 2009. Evolution, architecture and hierarchy of distributary deep-water deposits: a high-resolution outcrop investigation from the Permian Karoo Basin, South Africa. Sedimentology, 56, 2132–2154.

Pyles, D.R., Jennette, D.C., Tomasso, M., Beaubouef, R.T. and Rossen, C., 2010. Concepts learned from a 3D outcrop of a sinuous slope channel complex: beacon channel complex, Brushy Canyon Formation, West Texas, U.S.A. Journal of Sedimentary Research, 80, 67-96.

Schwarz, E., Arnott, R.W.C., 2007. Anatomy and evolution of a slope channel-levee complex set (Neoproterozoic Isaac Formation, Windermere Supergroup, southern Canadian Cordillera): implications for reservoir characterization. Journal of Sedimentary Research, 77, 89–109.

Selli, R., 1962. Il Paleogene nel quadro della geologia dell'Italia meridionale. Memorie della Società Geologica Italiana, 3 (7).

Stevenson, C.J., Jackson, C.A. L., Hodgson, D.M., Hubbard, S.M., Eggenhuisen, J.T., 2015. Deep-water sediment bypass. Journal of Sedimentary Research, 85, 1058-1081.

Stright, L., Stewart, J., Campion, K., Graham, S., 2014. Geologic and seismic modeling of a coarse-grained deep-water channel reservoir analog (Black's Beach, La Jolla, California). AAPG Bulletin, 98, 4, 695– 728.

Talling, P.J., Masson, D.G., Sumner, E.J., Malgesini, G., 2012. Subaqueous sediment density flows: Depositional processes and deposit types. Sedimentology, 59, 1937–2003.

Thurmond, J., Loseth, T., Rivenaes, J., Martinsen, O., Xu, X., Aiken, C., 2006. Using outcrop data in the 21st Century–New methods and applications, with example from the Ainsa Turbidite System, Ainsa, Spain. Deep-Water Outcrops of the World Atlas, Tulsa, OK, American Association of Petroleum Geologists Special Publication CD-ROM.

Vezzani, L., Festa, A., Ghisetti, F. C., 2010. Geology and tectonic evolution of the Central-Southern Apennines, Italy. Geological Society of America Special Papers, 469, 1-58.

Wynn, R.B., Talling, P.J., Amy, L., 2005. Imaging bed geometry and architecture of massive sandstones in the Fontanelice Channels, Italian Apennines, using new digiscoping techniques. Sedimentary Geology, 179, 153-162.

Figure Captions

Figure 1. Map of the eastern sector of the Gorgoglione Flysch Formation in the Southern Apennines of Italy (from Giannandrea et al., 2016, modified).

Figure 2: GigaPan® imagery methods. A) Location of 4 GigaPan® images used at medium range for the analysis of the stratigraphic section (1 and 2) and at close range for selected intervals (3 and 4). B) Tripod mounted GigaPan recording the outcrop. B) Photo stitching procedure using GigaPan® Stitch software. D and E) Resulting GigaPan® images of the Santa Maria Section.

Figure 3. Photogrammetry procedures for the construction of photorealistic 3D models from ground based and aerial photo sets, using Agisoft Photoscan®. A) Un-oriented ground-based photos collected at 1- 2 meters from the outcrop processed into a point cloud. B) Same photo set from A, processed as a solid object. C, D) Input aerial images for creation of aerial based 3D model. E) Aligned aerial photos and rendered dense point cloud showing the helicopter flight path and location of input photos. F) Fully rendered 3D model showing location of inset area in figure 5A.

Figure 4. The high-resolution GigaPan® technique. A) Full outcrop GigaPan. B) Selected section of the image A seen under medium zoom. B) Selected section of image A under full zoom showing a 1.5 meter Jacob staff for scale.

Figure 5. The Santa Maria section. A) Aerial image of section exposed along a staircase above the town of Castelmezzano rotated approximately 45 degrees to correct bedding to horizontal. B) Annotated outcrop section. C) Close-up illustration of the section, showing facies distribution.

Figure 6. Annotated composite GigaPan image showing measured stratigraphic sections, facies, and paleoflow data

Figure 7. Outcrop photographs of Facies Association A. A) Santa Maria Section indicating locations for facies photos in figs 7 & 8 B) Thick bedded sandstones of facies A1. C) Close-up view of the plane parallel laminated sandstone beds of facies A1. D) Heterolithic packages of interbedded fine-grained sandstones and mudstones (facies A2); 0.3-m-long hammer for scale. E) Contorted sandstone bed of facies A3, showing dewatering structures and minor brittle faulting (7.8 x 7.1 cm compass for scale).

Figure 8. Outcrop photographs of Facies Association B. A) Mixed extrabasinal and mud-clast rich conglomeratic deposits of facies B1, characterizing the channel axis (1 m logging staff for scale). B) Mud clast rich conglomerates of facies B1 in the channel off-axis (2 m Jacob's staff for scale). C) Exposed basal erosional surface, showing flute casts, grooves and rotated rose diagram showing paleoflow distribution. D) Massive structureless sandstones of facies B2, with thin mud clasts horizons marking amalgamation surfaces. E) Cross-laminated sandstones of facies B3, overlying amalgamated sandstones of facies B2.

Figure 9. *A)* Schematic cross-section of the Santa Maria Channel, showing the different portions of the channel (axis / off-axis / margin) and related facies distribution. Abundant mixed

extraformational conglomerates and intrabasinal mudclasts characterize the channel axis (see Fig. 8A). The amount of extraformational elements considerably decreases in the channel off-axis, where facies B1 is almost entirely constituted of mudclasts (see Fig. 8B). The channel margin is marked by the absence of lag deposits, with predominant cross-laminated sandstones (facies B3) and amalgamated structureless sandstones (facies B2), directly overlying the basal erosional surface. *B)* Block diagrams describing the evolutionary model for the Santa Maria channel-lobe system (see text for a detailed discussion). The background sedimentation is represented by mud-prone heterolithic thin bedded deposits that characterize the upper part of the Gorgoglione Flysch succession.

Table 1. Facies and facies associations

Table 1
Lithofacies and Facies Associations

*Interpretations and architectural elements after Bouma 1962, Lowe 1982

Facies Association A

Lithofacies	**Lithology**	**Grain size and sorting**	**Basal Surfaces**	**Sedimentary Structures**	**Thickness**	**Paleoflow**	**Interpretations***	**Patterns of occurance**
Thick Bedded Sandstone (A1)	Sandstone	Medium to coarse grained	Sharp basal contact	Massive, normal grading and plane parallel laminations. Locally crossebedded.	20- 50 cm	SW-SE	Ta -Tb Bouma intervals deposited by high density turbidity currents in depositional lobes.	Occurs as alternating packages of Facies A1 and Facies A2 which are overlain and truncated by an upper irregular erosional surface. Facies A3 can be found within A1 beds passing laterally from chaotic beds gradually transitioning into regularlly bedded A1 inctervals.
Mud Rich Heterolithic (A2)	Dark grey mudstone and siltstone	Mudstone and fine grained sands	Gradational	Massive and minor plane parallel laminations.	0.5 - 1 m	NA	Deposited on lobe fringe environments, passes laterally into thicker and coarser deposits.	
Chaotic Bedded Heterolithic (A3)	Sandstone and mudstone	Medium to coarse grained sandstone	Sharp base marked by detachment surface	Convuluted and chaotic bedding with folds, minor thrusts and dewatering structures.	~1 m	NA	Mass wasting resulting in detachment and dislocation of slumps towards a downdip location causing internal deformation of strata in both britle and ductile senses.	

Facies Association B

Lithofacies	**Lithology**	**Grain size and sorting**	**Basal Surfaces**	**Sedimentary Structures**	**Thickness**	**Paleoflow**	**Interpretations***	**Patterns of occurance**
Coarse Grained Conglomerate (B1)	Oligomictic conglomerate and sandstone	Very coarse, poorly sorted conglomerate in coarse sand matrix	Sharp and irregular erosional with underlying strata	Normal vertical grading with loading structures	3-5 m	S/SE	Lowe Division R3. Channel lag sediments deposited during periods of sediment bypass.	Occurs as a 20 - 30 meter package marked by a sharply erosional lower bounding surface with a terraced geometry stepping upwards from a proximal portion which truncates underlying stratigraphy. Lower units found as Facies B1 passing gradationally upwards into Facies B2 marked by the loss of large agnular clasts and transition into massive sands with mud rip up clasts. Facies B2 passes upwards gradationally into overlying Facies B3 marked by the loss of mud rip up clasts and transition into strongly dune
Amalgamated Sandstone (B2)	Sandstone	Medium to coarse grained sand	Sharp surface indicated by aligned mud rip-up clasts	Massive with subtle normal grading and aligned mud rip up clasts	~1 m	NA	Deposition from rapidly collapsing high density turbidity currents during filling phase of channel evolution.	
Crossbedded Sandstone (B3)	Sandstone	Medium to coarse grained sand with sparse pebbles	Gradational with underlying strata	Dune-scale cross bedding	1-3 m	SW	Sediment reworking by overpassing turbidity currents.	

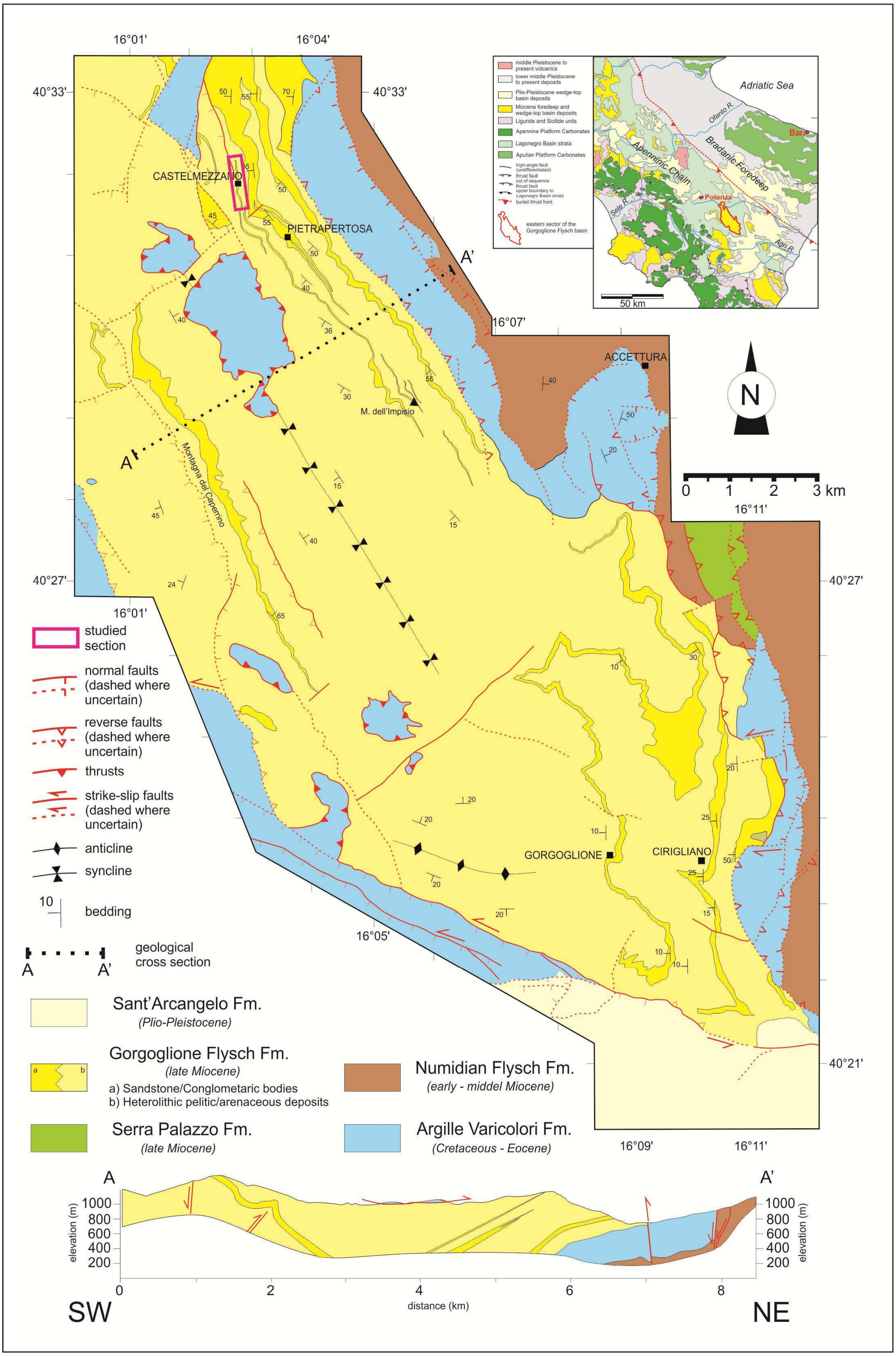
16°01'
16°04'
40°33'
40°33'
CASTELMEZZANO
PIETRAPERTOSA
A'
A
16°07'
ACCETTURA
M. dell'Impisio
Montagna del Caperrino
N
0 1 2 3 km
16°11'
40°27'
40°27'
16°01'
GORGOGLIONE
CIRIGLIANO
16°05'
40°21'
16°09'
16°11'
Adriatic Sea
Ofanto R.
Bari
Bradanic Foredeep
Apenninic Chain
Potenza
Sele R.
Agri R.
50 km
middle Pleistocene to present volcanics
lower middle Pleistocene to present deposits
Plio-Pleistocene wedge-top basin deposits
Miocene foredeep and wedge-top basin deposits
Liguride and Sicilide units
Apennine Platform Carbonates
Lagonegro Basin strata
Apulian Platform Carbonates
eastern sector of the Gorgoglione Flysch basin
studied section
normal faults (dashed where uncertain)
reverse faults (dashed where uncertain)
thrusts
strike-slip faults (dashed where uncertain)
anticline
syncline
bedding
geological cross section
Sant'Arcangelo Fm.
(Plio-Pleistocene)
Gorgoglione Flysch Fm.
(late Miocene)
a) Sandstone/Conglometaric bodies
b) Heterolithic pelitic/arenaceous deposits
Serra Palazzo Fm.
(late Miocene)
Numidian Flysch Fm.
(early - middel Miocene)
Argille Varicolori Fm.
(Cretaceous - Eocene)
elevation (m)
distance (km)
SW
NE

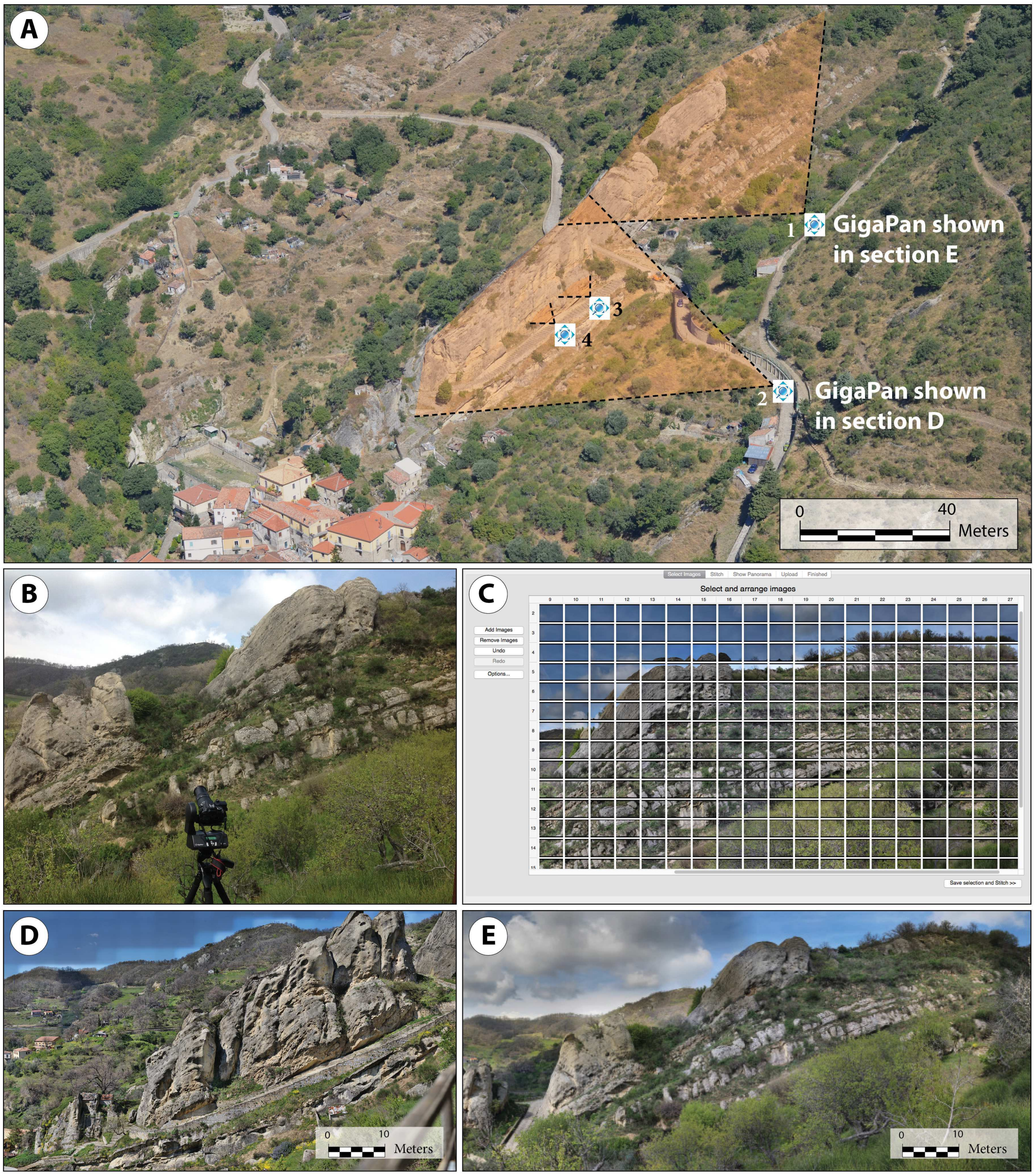
A
1
GigaPan shown in section E
3
4
2
GigaPan shown in section D
0
40
Meters
B
C
Select and arrange images
Add Images
Remove Images
Undo
Redo
Options...
D
0
10
Meters
E
0
10
Meters


A
B
C
0
10
Meters
Medium Zoom
Full Zoom

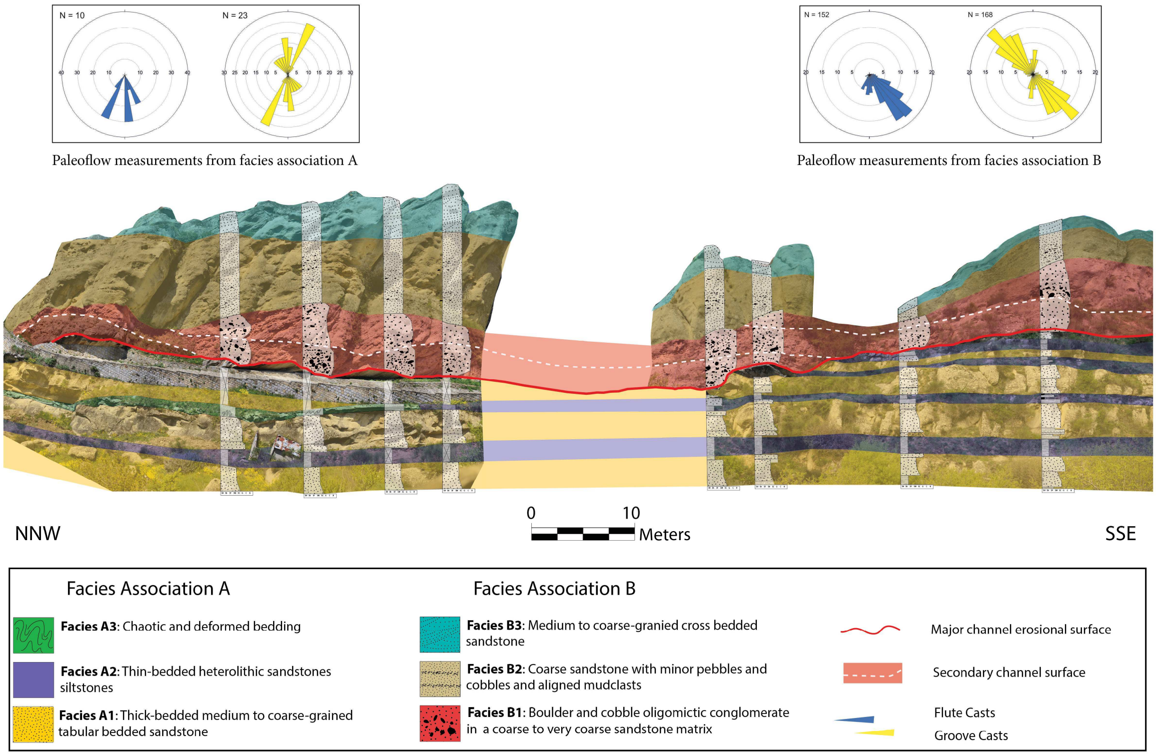
N = 10
N = 23
Paleoflow measurements from facies association A
N = 152
N = 168
Paleoflow measurements from facies association B
NNW
0
10
Meters
SSE
Facies Association A
Facies A3: Chaotic and deformed bedding
Facies A2: Thin-bedded heterolithic sandstones siltstones
Facies A1: Thick-bedded medium to coarse-grained tabular bedded sandstone
Facies Association B
Facies B3: Medium to coarse-granied cross bedded sandstone
Facies B2: Coarse sandstone with minor pebbles and cobbles and aligned mudclasts
Facies B1: Boulder and cobble oligomictic conglomerate in a coarse to very coarse sandstone matrix
Major channel erosional surface
Secondary channel surface
Flute Casts
Groove Casts

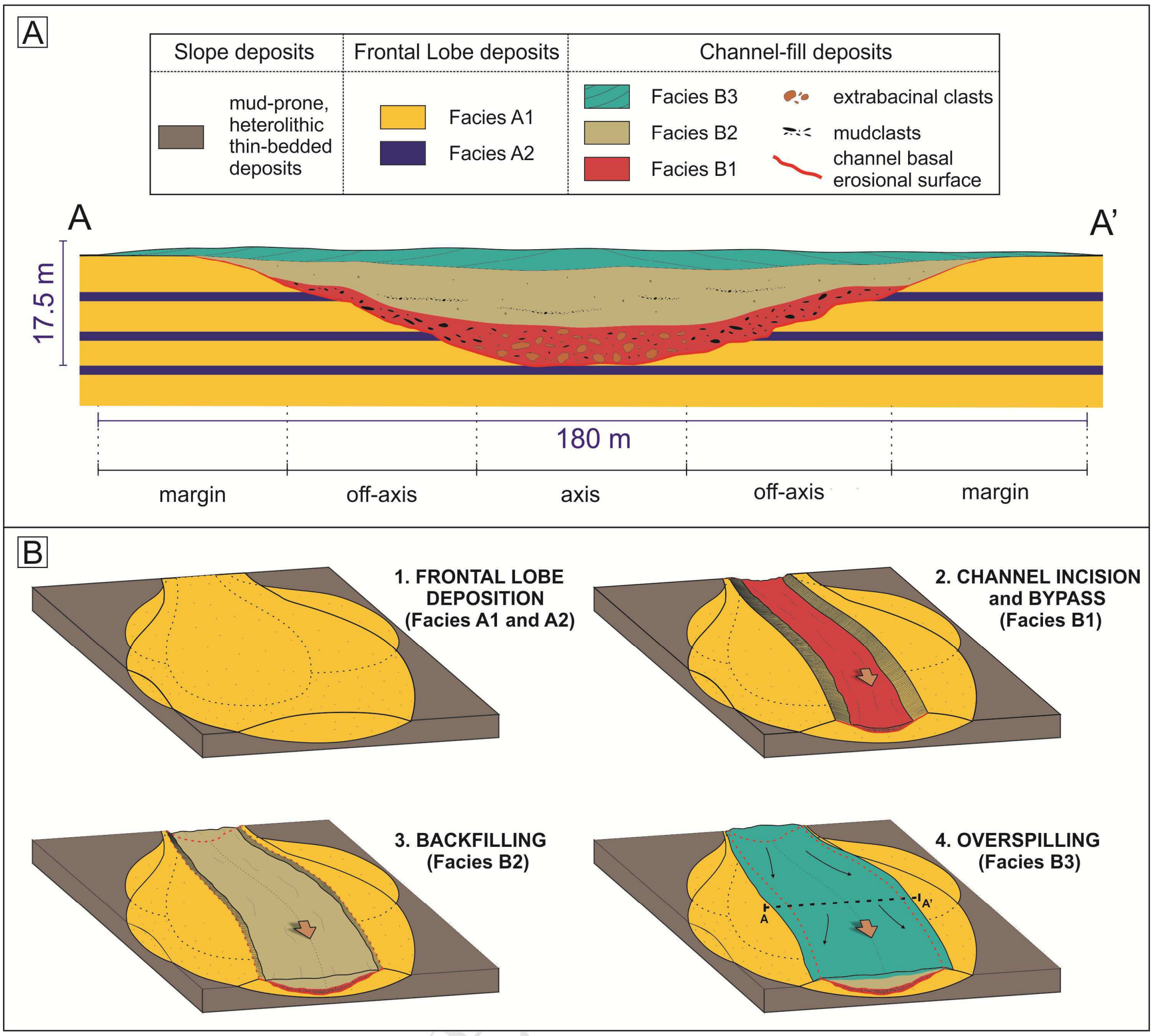
A
Slope deposits
Frontal Lobe deposits
Channel-fill deposits
mud-prone, heterolithic thin-bedded deposits
Facies A1
Facies A2
Facies B3
Facies B2
Facies B1
extrabacinal clasts
mudclasts
channel basal erosional surface
A
A'
17.5 m
180 m
margin
off-axis
axis
off-axis
margin
B
1. FRONTAL LOBE DEPOSITION (Facies A1 and A2)
2. CHANNEL INCISION and BYPASS (Facies B1)
3. BACKFILLING (Facies B2)
4. OVERSPILLING (Facies B3)
A
A'

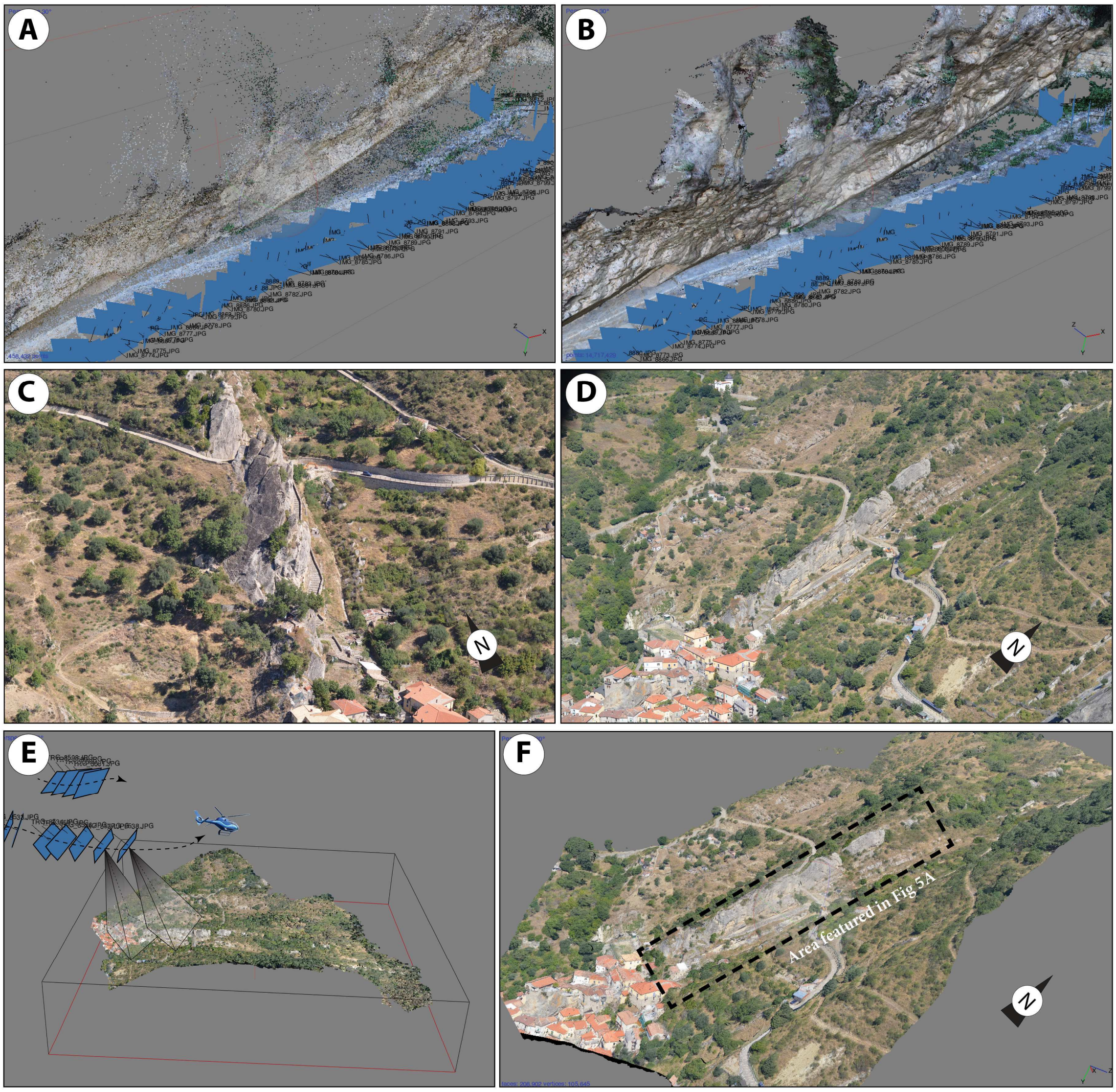
A
B
C
D
E
F
Area featured in Fig 5A
N

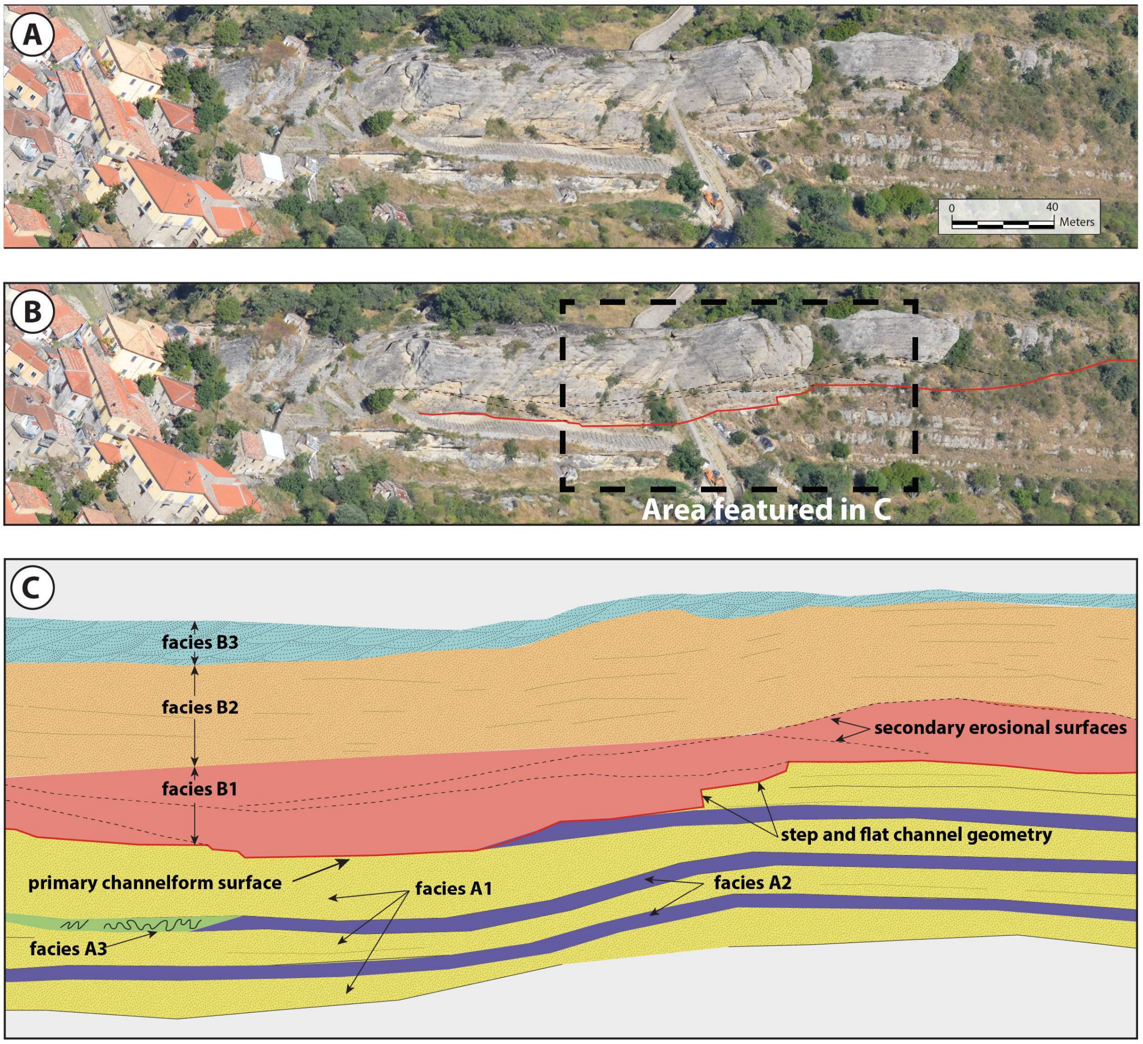
A
0
40
Meters
B
Area featured in C
C
facies B3
facies B2
facies B1
secondary erosional surfaces
step and flat channel geometry
primary channelform surface
facies A1
facies A2
facies A3

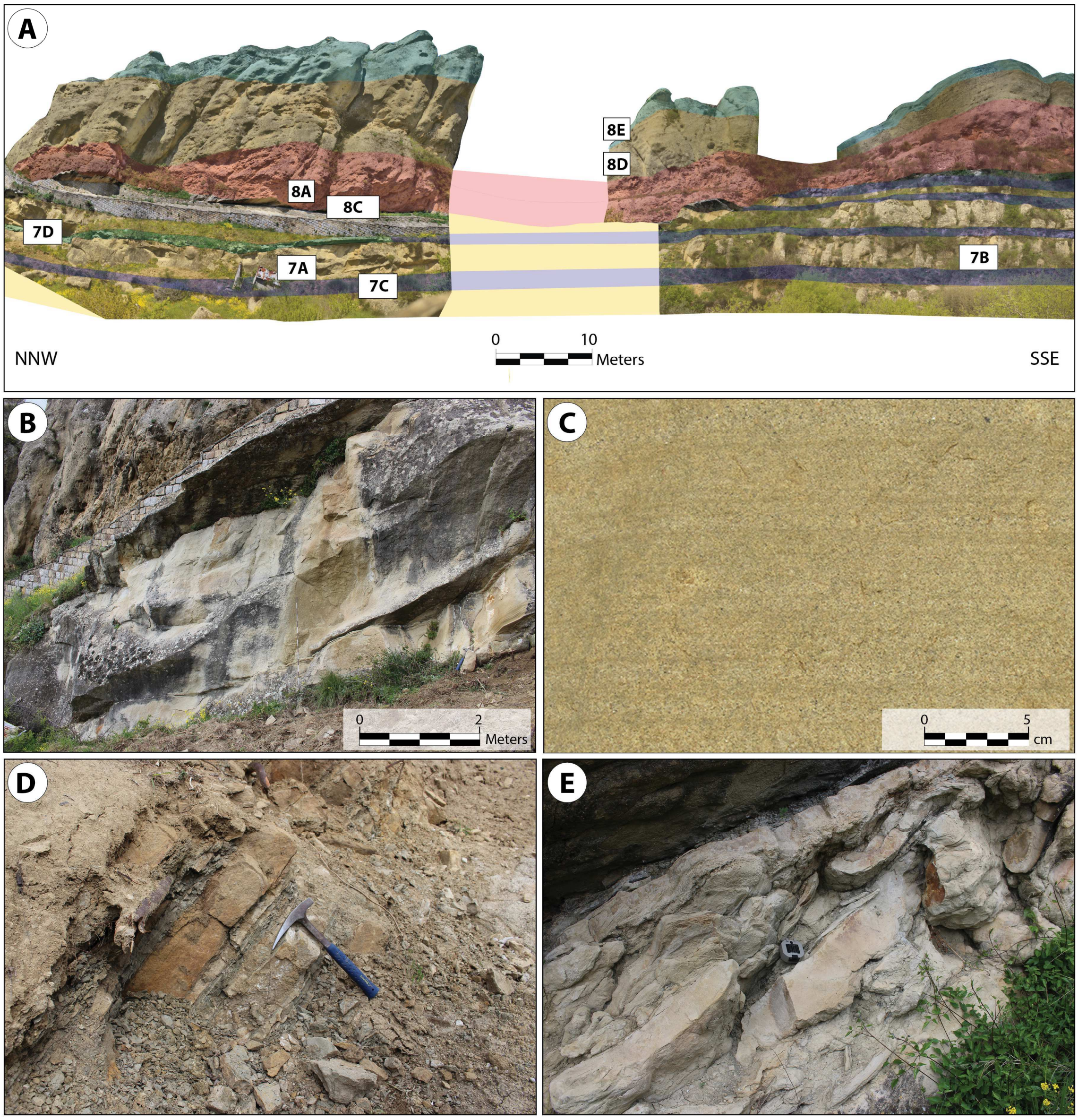
A
8E
8D
8A
8C
7D
7A
7C
7B
NNW
0
10
Meters
SSE
B
0
2
Meters
C
0
5
cm
D
E

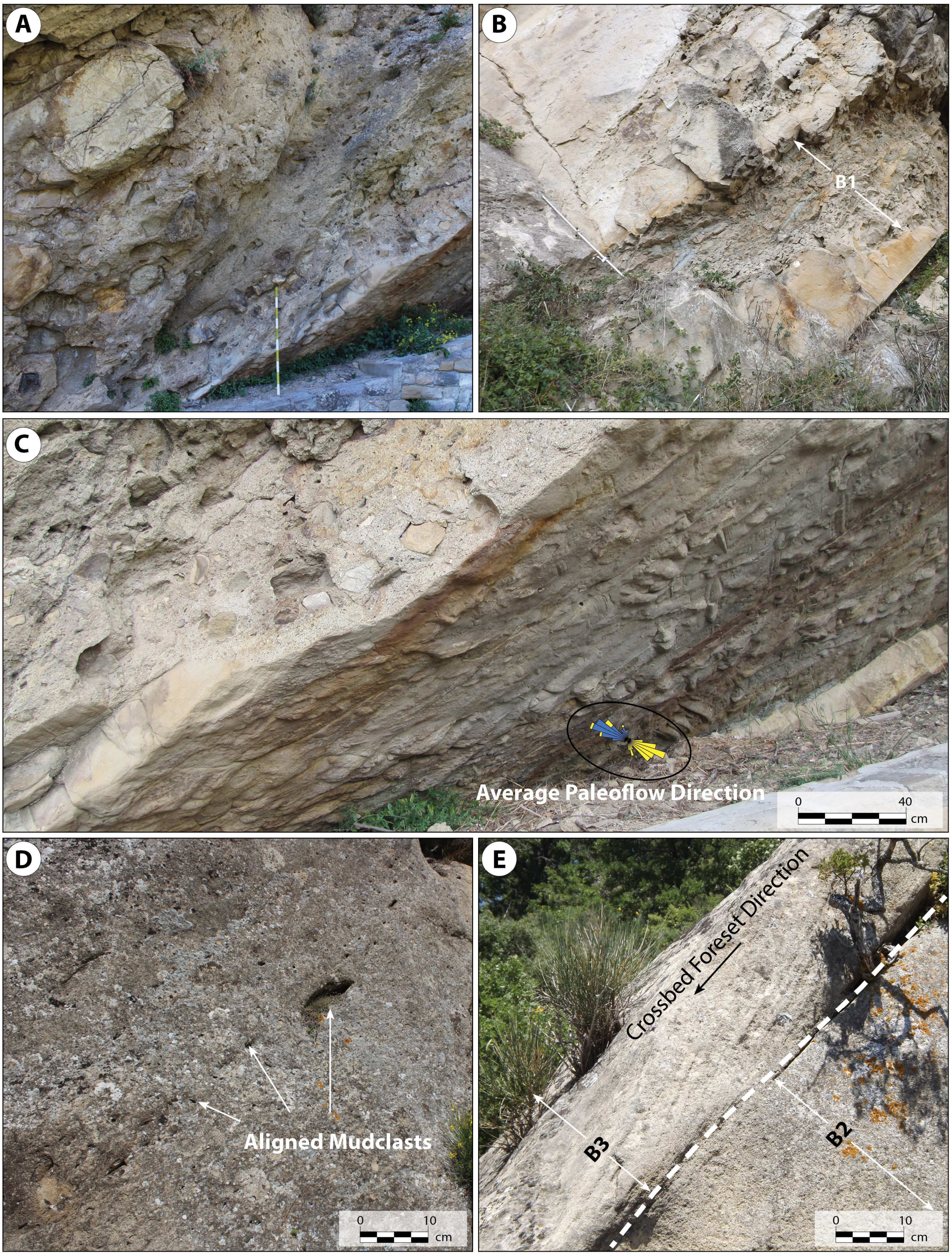
A
B
B1
C
Average Paleoflow Direction
0
40
cm
D
Aligned Mudclasts
0
10
cm
E
Crossbed Foreset Direction
B3
B2
0
10
cm

Highlights

Channelized turbidite succession was analyzed using standard field methods integrated with new digital field techniques using a GigaPan imagery system and 3D photogrammetry.

New methodologies for creating digital outcrop reconstructions can supplement physical data for enhanced facies characterization of bed-scale architecture and facies distribution.

Turbidite channel-lobe system at the Santa Maria section of the Gorgoglione Flysch Formation represents the full lifespan of a slope turbidite channel from inception to filling and eventual abandonment.

Facies characterization, stratigraphic correlations and reconstruction of the depositional architecture has been substantially enhanced by the use of emerging digital techniques for geological data collection.